Proceedings of the Seventh International Conference on
Railway Technology: Research, Development and Maintenance
Edited by: J. Pombo
Civil-Comp Conferences, Volume 15, Paper 11.15
Civil-Comp Press, Edinburgh, United Kingdom, 2026
ISSN: 2753-3239, doi: 10.4203/ccc.15.11.15

Nonlinear Dynamic Analysis of HTS maglev Train Under Guideway Disturbances

G. Migliaccio[1], F. D'Annibale[2], G. Antonini[3], H. Li[4], Z. Deng[4], W. Zhang[4] and G. D'Ovidio[2]

[1] National Group for Mathematical Physics, Italia
[2] Department of Civil, Construction-Architectural and Environmental Engineering (DICEAA), University of L'Aquila, Italy
[3] Department of Industrial and Information Engineering and Economics, University of L'Aquila, Italy
[4] Research Center for Super-High-Speed Evacuated Tube Maglev Transport, Southwest Jiaotong University, Chengdu, China

Abstract

High-temperature superconducting (HTS) magnetic levitation systems exhibit contactless levitation with strongly nonlinear force–displacement behavior and low inherent damping. This work examines the nonlinear dynamics of an HTS maglev train, with particular focus on the engineering implications of its sensitivity to guideway-induced disturbances. To support design-oriented analytical investigations, a reduced-order dynamic model is adopted that preserves the essential nonlinear characteristics of the levitation force. The Multiple Scales Method (MSM) provides analytical expressions for the system's vertical oscillations. Based on the authors' recent works, this framework enables an analytical evaluation of the influence of key design parameters on the system dynamics. The analysis reveals resonance conditions arising from the interaction between external disturbances and nonlinear levitation effects, which may lead to excessive vibration levels if not properly addressed at the design stage. Numerical simulations based on direct time-domain integration show good agreement with the analytical solutions over a broad range of operating conditions. Overall, the presented approach offers an efficient, design-oriented tool for parameter optimization and the mitigation of vibration-related issues in HTS maglev systems.

Keywords: magnetic levitation, vibration control, damping design, multiple time scales, resonances, analytical methods

1 Introduction

Magnetic levitation (maglev) systems are at the forefront of modern railway technology. Since the introduction of magnetic levitation, significant advances have been achieved in its application to transportation [1]. Maglev trains, whether in operation or under development, include superconducting electrodynamic suspension [2], electromagnetic suspension [3,4], and high-temperature superconducting (HTS) magnetic levitation [5]. Among these, HTS magnetic levitation offers high energy efficiency, operational stability, and adaptability across a wide range of speeds, from low to ultra-high. However, its inherently weak damping makes it highly sensitive to external disturbances, such as mechanical and magnetic irregularities in the guideway, which can compromise stability and produce significant vibrations. Consequently, extensive research has focused on optimizing guideway configurations to improve overall system performance [6–9]. Most solutions employ a flat permanent magnet guideway (PMG). In contrast, the system described in [10] utilizes a V-shaped PMG, initially proposed by the University of L'Aquila in 2008, tested on the UAQ4 laboratory track, and later refined through numerical optimization [9, 11, 12] (see Figure 1).

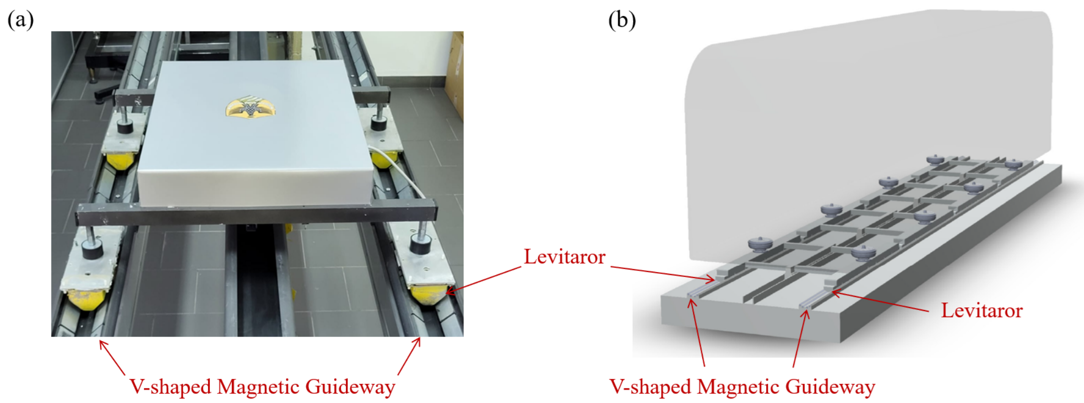

Figure 1: (a) Maglev system experimental setup with V-shaped levitators at the University of L'Aquila, and (b) schematic of a Maglev vehicle on the guideway, measuring 13 m in length, 3 m in width, 3.6 m in height, total weight 24,950 kg at full passenger capacity, empty weight 14,900 kg.

Building on prior collaborations between the University of L'Aquila (Italy) and Southwest Jiaotong University (China), this study examines a refined V-shaped PMG configuration incorporating a Halbach array. In this design, the vertical and horizontal components of the magnetic field generate levitation and guidance forces, respectively. These forces have been determined through numerical simulations [11, 12] as functions of the vehicle body's vertical and horizontal position. A full-scale HTS maglev system for urban transportation, employing this V-shaped levitation mechanism, is depicted in Figure 1(b). The vehicle consists of a body mechanically connected to four bogies via eight secondary suspensions, with each bogie containing four superconducting levitators and the stator of the linear motor.

The inherently low damping characteristics of the maglev system under study makes it highly susceptible to guideway-induced disturbances, which can adversely affect passenger comfort, system performance, and vehicle stability, potentially causing vibrations that compromise safety. Linear analysis is insufficient for assessing the impact of levitation model parameters on system dynamics. In practice, the large oscillations associated with resonance phenomena, common in many dynamical systems [13–16], are affected and can be mitigated by nonlinearities, such as the nonlinear characteristics of the levitation force outlined in [11, 12]. The present study analytically examines the influence of this nonlinearity on the dynamics and stability of the HTS maglev system using the Multiple Scales Method (MSM).

The paper is organized as follows. Section 2 introduces the reduced nonlinear dynamic model of the maglev system and presents an analytical investigation using the Method of Multiple Scales to assess the impact of key design parameters on the system's nonlinear dynamics. Section 3 presents the results of numerical simulations. Finally, conclusions and future perspectives are discussed in Section 4.

2 Analytical investigation

This section revisits and exploits the theoretical model presented in [16] to analyze the nonlinear dynamics and vertical oscillations of the HTS maglev system under study. The vehicle body moving along the PMG is modeled as a rigid body subjected to vertical disturbances, gravitational forces, and the levitation force. The governing equation of motion for the vertical oscillations of the system is

$$\ddot{x} + 2\mu\dot{x} + \omega^2 x + \kappa_2 x^2 + \kappa_3 x^3 + \mu_2 \dot{x}^2 + \mu_3 \dot{x}^3 = p\,\cos(\Omega t), \qquad (1)$$

where $x(t)$ denotes the vehicle's vertical displacement, ω is the system's natural frequency, and μ is the linear damping coefficient. The constants κ_2 and κ_3 correspond to the nonlinear elastic components of the levitation force, while μ_2 and μ_3 account for the nonlinear viscous contributions. Finally, p represents the amplitude of the external excitation per unit mass m of the vehicle body. Henceforth, the time dependence of variables (e.g., $x(t)$) is implied and omitted for brevity.

For a lightly damped, weakly nonlinear system governed by Equation (1), a small-amplitude excitation p can produce a relatively large response when the excitation frequency Ω approaches the system's natural frequency ω. Although analytical solutions to Equation (1) are generally unavailable, the effects of the levitation force nonlinearity, characterized by the parameters κ_2, κ_3, μ_2, and μ_3, on the system dynamics can be studied analytically using the Multiple Scales Method (MSM).

The first step of the MSM is the rescaling and expansion of the displacement field, $x(t) \to \varepsilon(x_0(t) + \varepsilon x_1(t) + \varepsilon^2 x_2(t) + ...)$, where $0 < \varepsilon \ll 1$ is a small bookkeeping parameter to be reabsorbed at the end of the procedure. The damping parameter and the amplitude of the forcing are also rescaled, $\mu \to \varepsilon^2\mu$, $p \to \varepsilon^3 p$. The frequency of the forcing is recast in the form $\Omega = \omega + \varepsilon^2\sigma$, where σ is a detuning parameter introduced to measure the nearness of Ω to ω. Independent time scales are introduced, $t_k = \varepsilon^k\, t$, $k = 0, 1, ...$ Consequently, the total time derivative is expressed in terms of partial derivatives with respect to the time scales t_k, in the form $\mathrm{d}/\mathrm{d}t = \mathrm{d}_0 + \varepsilon\, \mathrm{d}_1 + \varepsilon^2\, \mathrm{d}_2 + ...$, and $\mathrm{d}^2/\mathrm{d}t^2 = \mathrm{d}_0^2 + 2\varepsilon\, \mathrm{d}_0\mathrm{d}_1 + \varepsilon^2\, (\mathrm{d}_1^2 + 2\mathrm{d}_0\mathrm{d}_2) + ...$, where d_k stands for partial differentiation with respect to t_k. The perturbation equations of the MSM are finally derived by substitution in Equations (1) and collection of terms with the same power of ε. The first three *perturbation equations* are

$$\begin{aligned} &\mathrm{d}_0^2 x_0 + \omega^2 x_0 = 0, \\ &\mathrm{d}_0^2 x_1 + \omega^2 x_1 = -\, 2\mathrm{d}_1\mathrm{d}_0 x_0 - \kappa_2 x_0^2 - \mu_2(\mathrm{d}_0 x_0)^2, \\ &\mathrm{d}_0^2 x_2 + \omega^2 x_2 = -\, 2\mathrm{d}_1\mathrm{d}_0 x_1 - 2\mathrm{d}_2\mathrm{d}_0 x_0 - \mathrm{d}_1^2 x_0 - 2\mu\mathrm{d}_0 x_0 - 2\kappa_2 x_0 x_1 - \kappa_3 x_0^3 \\ &\qquad\qquad - 2\mu_2\mathrm{d}_0 x_0\,(\mathrm{d}_0 x_1 + \mathrm{d}_1 x_0) - \mu_3(\mathrm{d}_0 x_0)^3 + p\cos(\omega t_0 + \sigma t_2). \end{aligned} \tag{2}$$

The perturbation equations (2) must be solved sequentially, as described in [16]. The general solution to the zero-order perturbation equation (the so-called generating solution) takes the form

$$x_0 = A e^{i\omega t_0} + cc, \tag{3}$$

where $A(t_1, t_2, \dots)$ is an unknown complex amplitude that depends on the slow time scales t_1, t_2, etc. Substituting Equation (3) into the first-order perturbation equation (2) yields a nonhomogeneous differential equation in the unknown variable x_1

$$\mathrm{d}_0^2 x_1 + \omega^2 x_1 = -2i\omega\mathrm{d}_1 A e^{i\omega t_0} - \left(\kappa_2 - \mu_2\omega^2\right) A^2 e^{i2\omega t_0} - \left(\kappa_2 + \mu_2\omega^2\right) A\bar{A} + cc. \tag{4}$$

Time-diverging (secular) terms arising in the particular solution of the first-order perturbation equation (4) can be removed by imposing the solvability (or compatibility) condition $\mathrm{d}_1 A = 0$. Under this condition, the particular solution of the first-order perturbation problem becomes

$$x_1 = \frac{\kappa_2}{\omega^2}\left(-A\bar{A} + \frac{A^2}{3}e^{2i\omega t_0}\right) + \mu_2\left(-A\bar{A} - \frac{A^2}{3}e^{2i\omega t_0}\right) + cc. \tag{5}$$

This first-order solution (5) represents the first correction to the generating solution (3) and explicitly incorporates the effects of levitation nonlinearity through the parameters μ_2 and κ_2. Substituting both the generating solution (3) and the first-order solution (5) into the second-order perturbation equation (2) yields a nonhomogeneous differential equation in the unknown variable x_2, which is expressed as follows

$$\begin{aligned}\mathrm{d}_0^2 x_2 + \omega^2 x_2 = &- \left[2i\omega\left(\mathrm{d}_2 A + \mu A\right) - \frac{p}{2} e^{i\sigma t_2}\right] e^{i\omega t_0} \\ &- \left(3\kappa_3 - 3i\mu_3\omega^3 - \frac{10\kappa_2^2}{3\omega^2} - \frac{14\kappa_2\mu_2}{3}\right) A^2 \bar{A} e^{i\omega t_0} \\ &- \left(\kappa_3 + i\mu_3\omega^3 + \frac{2\kappa_2^2}{3\omega^2} - \frac{2\kappa_2\mu_2}{3}\right) A^3 e^{3i\omega t_0} + cc.\end{aligned} \tag{6}$$

The second-order solvability condition for equation (6) reads

$$2i\omega\left(\mathrm{d}_2 A + \mu A\right) + \left(3\kappa_3 - 3i\mu_3\omega^3 - \frac{10\kappa_2^2}{3\omega^2} - \frac{14\kappa_2\mu_2}{3}\right) A^2 \bar{A} = \frac{p}{2} e^{i\sigma t_2}. \tag{7}$$

By imposing the condition (7), a particular bounded solution of the second-order perturbation equation (6) is obtained in the form

$$x_2 = \left(\kappa_3 + i\mu_3\omega^3 + \frac{2\kappa_2^2}{3\omega^2} - \frac{2\kappa_2\mu_2}{3}\right) \frac{A^3}{8\omega^2} e^{3i\omega t_0} + cc. \tag{8}$$

By combining Equations (3), (5), and (8), and performing the inverse rescaling of the complex amplitude, $\varepsilon A \to A$, to reabsorb the perturbation parameter ε, the asymptotic expression for the state variable $x(t)$ can be written as

$$\begin{aligned}x(t) = &A e^{i\omega t_0} - \frac{\kappa_2}{\omega^2}\left(A\bar{A} - \frac{A^2}{3} e^{2i\omega t_0}\right) - \mu_2\left(A\bar{A} + \frac{A^2}{3} e^{2i\omega t_0}\right) + \\ &\left(\kappa_3 + i\mu_3\omega^3 + \frac{2\kappa_2^2}{3\omega^2} - \frac{2\kappa_2\mu_2}{3}\right) \frac{A^3}{8\omega^2} e^{3i\omega t_0} + cc + o(A^3).\end{aligned} \tag{9}$$

Equation (9) provides the asymptotic solution for the problem, once it is complemented by an expression for the complex amplitude A. This amplitude arises from the solvability conditions of the first- and second-order perturbation equations, combined within the asymptotic expansion of the total time derivative of A, namely, $\dot{A} = \varepsilon\left(\mathrm{d}_0 A + \varepsilon \mathrm{d}_1 A + \varepsilon^2 \mathrm{d}_2 A + ...\right)$. By combining these conditions and applying the inverse rescaling $\varepsilon A \to A$, $\varepsilon^2\mu \to \mu$, $\varepsilon^3 p \to p$, and $\varepsilon^2\sigma \to \sigma$, the following differential equation in the true time is obtained

$$\dot{A} + \left(\mu - i\alpha\left|2A\right|^2\right) A = -\frac{ip}{4\omega} e^{i\sigma t}. \tag{10}$$

where the coefficient α reflects the influence of the nonlinear levitation force through the parameters κ_2, μ_2, κ_3, and μ_3, and is defined as follows

$$\alpha = \frac{9\kappa_3\omega^2 - 9i\mu_3\omega^5 - 10\kappa_2^2 - 14\kappa_2\mu_2\omega^2}{24\omega^3}. \tag{11}$$

Equation (10) represents the Amplitude Modulation Equation (AME) corresponding to the weakly nonlinear differential equation (1). Its steady-state solutions describe the system's periodic motions, while, in general, the AME governs how the oscillation amplitude evolves over time. To solve Equation (10), the complex amplitude A is expressed in polar form, $2A(t) = a(t)e^{i\varphi(t)}$, introducing the real amplitude $a(t)$ and real phase $\varphi(t)$. Substituting this expression into Equation (10) yields

$$\begin{cases} \dot{a} + \mu a = \frac{p}{2\omega}\sin\theta, \\ a\dot{\theta} - \sigma a + \alpha a^3 = \frac{p}{2\omega}\cos\theta, \end{cases} \tag{12}$$

where the variable $\theta := \sigma t - \varphi$ has been introduced to rewrite the real form of the AME (12) as a set of autonomous ordinary differential equations.

The real form of Equation (9) can be expressed as follows

$$\begin{aligned} x(t) = {} & a\cos(\Omega t - \theta) + \frac{a^2}{6}\left[-3\left(\frac{\kappa_2}{\omega^2} + \mu_2\right) + \left(\frac{\kappa_2}{\omega^2} - \mu_2\right)\cos(2\Omega t - 2\theta)\right] \\ & + \frac{a^3}{32}\left[\left(\frac{\kappa_3}{\omega^2} + \frac{2\kappa_2^2}{3\omega^4} - \frac{2\kappa_2\mu_2}{3\omega^2}\right)\cos(3\Omega t - 3\theta) - \mu_3\omega\sin(3\Omega t - 3\theta)\right] \\ & + o(a^3). \end{aligned} \tag{13}$$

Steady-state motion occurs when $\dot{a} = \dot{\theta} = 0$. The corresponding constant steady-state amplitude, $a(t) = a_s$, is determined from Equations (12), yielding

$$\mu^2 a_s^2 + \left(\sigma - \alpha a_s^2\right)^2 a_s^2 = \left(\frac{p}{2\omega}\right)^2, \tag{14}$$

which constitutes an implicit equation for the steady-state amplitude a_s, and also

$$\begin{cases} \sin\theta_s = \frac{2\omega\mu}{p}a_s, \\ \cos\theta_s = -\frac{2\omega\sigma}{p}a_s + \alpha a_s^3, \end{cases} \tag{15}$$

which determine the corresponding steady-state value of $\theta(t)$, denoted as θ_s.

Equation (14), referred to as the amplitude-frequency equation, implicitly defines the steady-state amplitude a_s as a function of the system parameters, the forcing amplitude p, and the forcing frequency (through the detuning parameter σ). Once a_s is known, Equations (15), known as the phase-frequency equations, allow the determination of the steady-state phase, $\varphi_s(t) = \sigma t - \theta_s$.

Equation (13) shows that the leading term of the steady-state response is tuned exactly to the external excitation frequency, with a phase shift of θ relative to the excitation. The parameters κ_2 and μ_2 introduce a correction to the leading term, causing the response to be offset from $x = 0$, while the effects of κ_3 and μ_3 appear only as higher-order corrections.

It is important to note that the motion described by the analytical solution is physically meaningful (observable) only if it is stable. To assess the stability of the periodic solution (13), a small perturbation is introduced via the change of variables $a = a_s + \delta a$ and $\theta = \theta_s + \delta\theta$, where δa and $\delta\theta$ are small deviations from the steady state. Substituting these into Equations (12) and neglecting higher-order terms leads to the following linearized form of the AME

$$\begin{bmatrix} \delta\dot{a} \\ \delta\dot{\varphi} \end{bmatrix} = \begin{bmatrix} -\mu & \alpha a_s^3 - \sigma a_s \\ \frac{\sigma}{a_s} - 3\alpha a_s & -\mu \end{bmatrix} \begin{bmatrix} \delta a \\ \delta\varphi \end{bmatrix}. \tag{16}$$

By analyzing the eigenvalues of the linearized system matrix, it can be concluded that the steady-state motions of the system are stable if and only if the system parameters satisfy the following condition

$$\left(\sigma - 3\alpha a_s^2\right)\left(\sigma - \alpha a_s^2\right) + \mu^2 > 0. \tag{17}$$

Equation (17) defines a constraint on the system and forcing parameters that guarantees the stability of the steady-state motion when the forcing frequency Ω is close to the system's natural frequency ω. Numerical examples based on this analytical solution and confirming the existence and observability of the corresponding stable motions are presented in the following Section 3.

3 Numerical analysis

The levitation force parameters best fitting the levitation curve outlined in [11, 12] are $\mu = 0.0069, \mathrm{s}^{-1}$, $\omega = 33.4591, \mathrm{s}^{-1}$, and $\kappa_2 = 4.3741 \cdot 10^4, \mathrm{m}^{-1}\mathrm{s}^{-2}$, with the remaining parameters, κ_3, μ_2, and μ_3, set to zero. As noted, the system's weak damping renders it highly sensitive to external disturbances, potentially impacting performance, passenger comfort, and dynamic stability. The asymptotic solution derived in Section 2 is used to analyze the effects of these nonzero levitation parameters on the system's nonlinear dynamics. A numerical benchmark, obtained via direct time integration of the nonlinear equation of motion, is also provided for comparison.

The system considered here is subjected to an external excitation with amplitude $p = 0.1\,\mathrm{m\,s^{-1}}$ and frequency $\Omega = (1+\bar{\sigma})\,\omega$, close to the natural frequency ω. The relevant Amplitude-Frequency response (a_s–Ω) for $\bar{\sigma} \in (-0.1, 0.1)$, i.e., $\Omega/\omega \in (0.9, 1.1)$ are shown in Figure 2(a). The blue branches indicate stable solutions (stable limit cycles) predicted by the MSM, while the red dashed branches correspond to unstable solutions. For reference, the grey lines represent the frequency response of the linear system, obtained by neglecting the nonlinear terms in the levitation model.

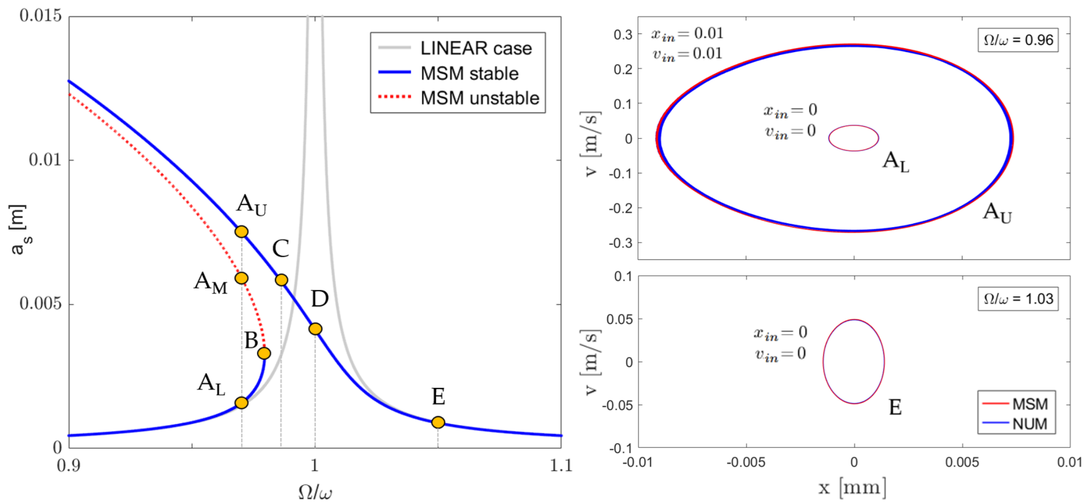

Figure 2: (a) Maglev amplitude-frequency response for $\mu = 6.9 \cdot 10^{-3}\,s^{-1}$, $\omega = 33.4591\,s^{-1}$, $\kappa_2 = 4.3741 \cdot 10^4\,m^{-1}s^{-2}$, $p = 0.1\,\mathrm{m}s^{-2}$; (b) Limit cycles obtained numerically (NUM) and analytically (MSM) at excitation frequencies $\Omega/\omega = (0.96, 1.03)$. Two limit cycles can be observed when $\Omega/\omega = 0.96$ (points A_L and A_U), only one for $\Omega/\omega = 1.03$ (point E).

Figure 2(a) highlights the effect of the levitation model nonlinearity on the system response, causing a leftward bending of the amplitude curve, which in turn leads to multi-valued regions in the frequency domain (frequency ranges where multiple steady-state solutions exist for a_s). For the system considered, this multi-valued behavior occurs for excitation frequencies Ω below point B, i.e. $\Omega < \Omega_B \simeq 0.978\,\omega$. Specifically, at $\Omega = \Omega_A = 0.96\,\omega$, three distinct solutions are observed: the first, at the lower blue branch (point A_L), corresponds to a stable motion; the second, on the middle red dashed branch (point A_M), is an unstable solution that is physically unattainable; the third, on the upper blue branch (point A_U), corresponds to another stable motion. In practice, the system may settle into either of the two stable solutions, depending on the initial state (initial position x_{in}, initial velocity v_{in}).

Figure 2(b) depicts the closed phase–space trajectories (limit cycles) reached by the system under different external excitations, with amplitude $p = 0.1\,\mathrm{m}s^{-2}$ and frequencies $\Omega/\omega = (0.96, 1.03)$. The blue curves denote the benchmark numerical solutions (NUM), whereas the red curves correspond to the analytical predictions obtained using the Multiple Scales Method (MSM). It is observed that, when $\Omega = 0.96\,\omega$, the system may converge to two distinct limit cycles. The smaller limit cycle, associated with point A_L in Figure 2, is reached when the system starts from the null initial condition $x_{in} = v_{in} = 0$. The larger limit cycle, corresponding to point A_U, is attained for the initial condition $x_{in} = 0.01\,\mathrm{m}$, $v_{in} = 0.01\,\mathrm{m}s^{-1}$. For $\Omega > 0.978\,\omega$, the resulting limit cycle is independent of the initial condition, in agreement with the frequency response curves shown in Figure 2(a).

The MSM limit cycles shown in Figure 2(b) are obtained from the MSM solution that includes the generating solution x_0 together with its first-order correction x_1. The contribution of higher-order terms in the asymptotic expansion, such as x_2 (the term proportional to a^3 in Equation (13)), can be neglected. In contrast, the first-order correction x_1 (proportional to a^2) is essential for accurately capturing the system's limit-cycle behavior. It is observed that when the system is subjected to an external harmonic excitation with frequency Ω close to the natural frequency ω, the MSM analytical solution (Equation (13)) exhibits excellent agreement with the results of the numerical integration of the nonlinear ordinary differential equation (1). The relative discrepancy between the analytical solution that includes the first-order correction x_1 and the benchmark numerical solution is of the order of 1%. This level of accuracy confirms that the MSM solution (13) constitutes a reliable efficient tool, capable of capturing the influence of the key design parameters of the maglev system, and can therefore be confidently employed for both system analysis and design purposes.

4 Conclusions and perspectives

The non-linear dynamics of the HTS maglev transit system under development at the University of L'Aquila has been investigated in the paper. Magnetic levitation enables high-speed, energy-efficient operation but is highly sensitive to external disturbances due to its inherently low damping. To analytically capture the system's complex behavior, the Multiple Scales Method (MSM) has been employed. The resulting analytical solutions are compact, physically insightful, and well suited for design and parametric studies, offering a computationally efficient alternative to full time-domain simulations. The analysis has highlighted resonance phenomena governed by damping, natural frequency, and nonlinear levitation force characteristics, which can strongly influence performance, stability, and safety. Numerical simulations based on direct integration of the nonlinear equations of motion have confirmed the accuracy of the MSM predictions over a broad range of operating conditions.

The model and analytical solutions developed in this study offer a valuable tool for guiding and supporting the design of the maglev system, as they explicitly capture the interdependencies between geometry, design constraints, and performance metrics related to the levitation force. This framework can facilitate efficient exploration of the design space, can help identify promising configurations for detailed evaluation, and can reduce dependence on computationally intensive simulations or costly experimental testing. Future work will focus on exploiting this analytical framework for design optimization. Additional research directions include: (i) analytical characterization of horizontal vibrations under the combined effects of magnetic guidance forces and external disturbances; (ii) investigation of coupling mechanisms between horizontal and vertical oscillations; (iii) development of effective vibration control strategies to enhance system damping; and (iv) design of energy-harvesting solutions to convert vibrational energy in this nonlinear system into usable electrical power for onboard applications, extending previous work limited to linear systems.

References

[1] G. Lanzara, G. D'Ovidio, et al., "Magnetic Levitation System Assessment from Transport Engineering Point of Wiew: Background and Future Prospects", Ingegneria Ferroviaria, Anno LXXVI, 7-8, 557-593, 2021.

[2] P. Holmer, "Bullet train", IEEE Spectr, 40, 8, 30-34, 2003.

[3] M. Ono, S. Koga, H. Ohtsuki, "Japan's superconducting MAGLEV train", IEEE Instrum. Meas. Mag., 5, 1, 9-15, 2002.

[4] H. Huang, H. Li, et al., "Advancements in dynamic characteristics analysis of superconducting electrodynamic suspension systems: Modeling, experiment, and optimization", Superconductivity, 11, 3, 51-65, 2024.

[5] J.R. Wang, M.Z. Wu, et al., "High-Tc superconductive vehicle for maglev model", Rare Met. Mater. Eng., 27, 4, 240-243, 1998.

[6] Z. Deng, W. Zhang, et al., "A High-Temperature Superconducting MAGLEV Ring Test Line Developed in Chengdu, China", IEEE Transactions on Applied Superconductivity, 26, 6, 1-8, 2016.

[7] L. Schultz, O. de Haas, et al., "Superconductively levitated transport system — The SupraTrans project", IEEE Transactions on Applied Superconductivity, 15, 2, 2301-2305, 2005.

[8] G. Sotelo, R.A.H. De Oliveira, et al., "A full scale superconducting magnetic levitation (MAGLEV) vehicle operational line", IEEE Transactions on Applied Superconductivity", 25, 3, 3601005, 2015.

[9] G. Lanzara, G. D'Ovidio, F. Crisi, "UAQ4 levitating train: Italian MAGLEV transportation system", IEEE Vehicular Technology Magazine", 9, 71-77, 2014.

[10] G. D'Ovidio, F. Crisi, G. Lanzara, "Design and optimization of UAQ4 experimental MAGLEV module", Materials Science Forum, 670, 42-47, 2011.

[11] L. Gao, Z. Deng, et al., "High-Temperature Superconducting Magnetic Levitation with the Halbach array and V-shaped combined permanent magnet guideway", IEEE Transactions on Applied Superconductivity, 34, 7, 1-8, 2024.

[12] Y. Yuan, L. Gao, et al., "Dynamics of a HTS Pinning MAGLEV System on a Stability-Enhanced V-Shaped PMG for Urban Transit", IEEE Transactions on Applied Superconductivity, 35, 8, 1-9, 2025.

[13] A.H. Nayfeh, D.T. Mook, "Nonlinear oscillations", Wiley-VCH Verlag GmbH & Co. KGaA, Weinheim, Germany, 2008.

[14] A.H. Nayfeh, "Perturbation methods", Wiley-VCH Verlag GmbH & Co. KGaA, Weinheim, Germany, 2000.

[15] G. Migliaccio, M. Ferretti, et al., "Analytical prediction of the dynamics of beams travelled by moving forces and external resonance phenomena", Journal of Sound and Vibrations, 593(22), 118656, 2024.

[16] G. Migliaccio, F. D'Annibale, et al., "A multiple scales approach to analyze the nonlinear dynamics of the high-temperature superconducting magnetic levitation train", International Journal of Non-Linear Mechanics, 180, 105268, 2026.